

STANDARD SOLAR NEUTRINOS

ARNON DAR AND GIORA SHAVIV

Department of Physics and Asher Space Research Institute, Technion-Israel Institute of Technology, Haifa 32000, Israel;
arnon@physics.technion.ac.il gioras@physics.technion.ac.il

Received 1995 September 14; accepted 1996 March 12

ABSTRACT

We describe in detail an improved standard solar model that has been used to calculate the fluxes of standard solar neutrinos. It includes pre-main-sequence evolution, element diffusion, partial ionization effects, and all the possible nuclear reactions between the main elements. It uses updated values for the initial solar element abundances, the solar age, the solar luminosity, the nuclear reaction rates, and the radiative opacities. Neither nuclear equilibrium nor complete ionization are assumed. The calculated solar neutrino fluxes are compared with published results from the four solar neutrino experiments. The calculated ^8B solar neutrino flux is consistent, within the theoretical and experimental uncertainties, with the solar neutrino observations at Homestake and Kamiokande. The observations suggest that the ^7Be solar neutrino flux is much smaller than that predicted. However, conclusive evidence for the suppression of the ^7Be solar neutrino flux will require experiments like BOREXINO and HELLAZ. If the ^7Be solar neutrino flux is suppressed, it still can be due either to standard physics reasons or neutrino properties beyond the standard electroweak model. Only future neutrino experiments, such as SNO, Superkamiokande, BOREXINO, and HELLAZ, will be able to show that the solar neutrino problem is a consequence of neutrino properties beyond the standard electroweak model.

Subject headings: elementary particles — nuclear reactions, nucleosynthesis, abundances — Sun: interior

1. INTRODUCTION

The Sun is a typical main-sequence star that generates its energy by fusion of protons into helium nuclei through the p - p and CNO nuclear reaction chains (Bethe 1939). These reactions also produce neutrinos. These neutrinos have been detected on Earth in four pioneering solar neutrino experiments, the radiochemical chlorine experiment at Homestake (Cleveland et al. 1995, and references therein), the electronic light water Cerenkov experiment at Kamioka (Suzuki 1995, and references therein), and the two radiochemical Gallium experiments, GALLEX at Gran Sasso (Anselmann et al. 1995a, 1995b and references therein) and SAGE at the Baksan (Abdurashitov et al. 1995, and references therein). They provide the most direct evidence that the Sun generates its energy via fusion of hydrogen into helium. However, it has been claimed (e.g., Bahcall 1995; Hata et al. 1994) that all four experiments measured solar neutrino fluxes significantly smaller than those predicted by standard solar models (SSMs) (e.g., Bahcall & Ulrich 1988; Turck-Chieze et al. 1988; Sackman et al. 1990; Bahcall & Pinsonneault 1992, hereafter BP92; Turck-Chieze & Lopes 1993, hereafter TL93; Castellani et al. 1994; Kovetz & Shaviv 1994; Christensen-Dalsgaard 1994; Shi et al. 1994; Bahcall & Pinsonneault 1995, hereafter BP95; see, however, Dar & Shaviv 1994, hereafter DS94; Shaviv 1995; Dzitko et al. 1995).

The Homestake chlorine experiment has been collecting data since 1970. Based on 25 years of observations, Cleveland et al. (1995) have recently reported an average ^{37}Ar production rate in ^{37}Cl of

$$\text{Rate (Chlorine)} = 2.55 \pm 0.17(\text{stat}) \pm 0.18(\text{syst}) \text{ SNU} \quad (1)$$

(where 1 SNU = 10^{-36} s^{-1} captures per atom) by solar neutrinos above the 0.814 MeV threshold energy for the reaction $\nu_e + ^{37}\text{Cl} \rightarrow e^- + ^{37}\text{Ar}$. It is $32\% \pm 5\%$ of the $8.1^{+1.0}_{-1.2}$ SNU predicted by the SSM of, e.g., BP92.

Kamiokande II and III observed electron recoils, with energies first above 9 MeV and later above 7 MeV, from

elastic scattering of solar neutrinos on electrons in water. Their 5.4 year data show a spectrum consistent with ^8B solar neutrino flux of (Suzuki 1995)

$$\phi_{\nu_e} = [2.9 \pm 0.2(\text{stat}) \pm 0.3(\text{syst})] \times 10^6 \text{ cm}^{-2} \text{ s}^{-1}, \quad (2)$$

which is $51\% \pm 9\%$ of that predicted by the SSM of BP92.

GALLEX, the European gallium experiment at the Gran Sasso underground laboratory, measured a ^{71}Ge production rate by solar neutrinos in ^{71}Ga of (Anselmann et al. 1995a)

$$\text{Rate (Gallium)} = 79 \pm 10(\text{stat}) \pm 6(\text{syst}) \text{ SNU}, \quad (3)$$

through the reaction $\nu_e + ^{71}\text{Ga} \rightarrow e^- + ^{71}\text{Ge}$, whose threshold energy is 233 keV. This rate is $60\% \pm 10\%$ of the 131.5^{+7}_6 SNU predicted by the SSM of BP92.

SAGE, the Soviet-American Gallium Experiment in the Baksan underground laboratory, reported (Abdurashitov et al. 1995) an average ^{71}Ge production rate by solar neutrinos in ^{71}Ga of

$$\text{Rate (Gallium)} = 74^{+13}_{-12}(\text{stat})^{+5}_{-5}(\text{syst}) \text{ SNU}, \quad (4)$$

during 1990–1993, which is consistent with the rate reported by GALLEX. It is $56\% \pm 11\%$ of the 131.5^{+7}_6 SNU predicted by the SSM of BP92.

These discrepancies between the observations and the predictions have become known as the solar neutrino problem(s). Three types of solutions to these solar neutrino problems have been investigated:

1. *Terrestrial solutions.*—Perhaps the accuracy of the results of the solar neutrino experiments has been overestimated, and unknown systematic errors are largely responsible for the solar neutrino problem.

2. *Astrophysical solutions.*—Perhaps the standard solar models do not provide sufficiently accurate description of the present-day Sun and/or the neutrino producing reactions in the Sun.

3. *Particle physics solutions.*—Perhaps nonstandard neutrino properties beyond the standard model are responsible for the solar neutrino problem.

The chances that possibility (1) is responsible for the solar neutrino problem have been reduced greatly by the GALLEX chromium source experiment performed last year (Anselmann et al. 1995b). This experiment is the first full demonstration of the reliability of the radiochemical technique for the detection of solar neutrinos. In particular, it excludes the possibility of any unidentified important sources of systematical errors, such as hot atom chemistry, in the radiochemical experiments. However, we will argue that terrestrial solutions to the solar neutrino problem have not been ruled out. In particular, the capture rate of solar neutrinos near threshold in ^{37}Cl and in ^{73}Ga may be significantly smaller than currently used for predicting SNU's (see § 7). We note also that although Kamiokande, the electronic water Cerenkov experiment, has definitely observed excess events pointing toward the Sun (Suzuki 1995), it has not been calibrated yet with a known neutrino source. Such a direct calibration is highly desirable, since Kamiokande has the formidable task of singling out solar neutrino events with an expected rate of the order of one per day in a fiducial volume of 680 tons of highly purified water, in which the total trigger rate of the detector for electron energy greater than 7 MeV is still 150,000 per day.

It should be noted also that the joint observations of Homestake and Kamiokande appear to be supported by the results of the gallium experiments (Dar 1993). Namely, both the joint results from Homestake and Kamiokande and the results from GALLEX and SAGE seem to indicate that the ^7Be solar neutrino flux is much smaller than that predicted by the SSMs (e.g., Dar 1993; Hata et al. 1994; Berezinsky 1994; Kwong & Rosen 1994; Parke 1995). In fact, the signals observed by GALLEX and SAGE can be predicted accurately from the observed solar luminosity and the solar neutrino observations of Homestake and Kamiokande (Dar 1993).

If the Sun derives its energy from fusion of hydrogen into helium, and if it is in a steady state in which its nuclear energy production rate equals its luminosity, then the total solar neutrino flux at Earth is given by (e.g., Dar & Nussinov 1992)

$$\phi_{\nu_{\odot}} = \frac{2L_{\odot}}{Q - 2\bar{E}_{\nu}} \frac{1}{4\pi D^2} \approx 6.51 \times 10^{10} \text{ cm}^{-2} \text{ s}^{-1}, \quad (5)$$

where $D \approx 1.496 \times 10^{13}$ cm is the distance to the Sun, $Q = 26.733$ MeV is the energy released when four protons fuse into helium, and the average energy of solar neutrinos has been approximated by $\bar{E}_{\nu}(p-p) = \Sigma E_{\nu} \phi_{\nu} / \Sigma \phi_{\nu} \approx 0.265$ MeV, the average energy of the $p-p$ neutrinos that dominate the sum rule. If the pep and CNO contributions to the solar neutrino flux are ignored, then

$$\phi_{\nu_{\odot}} \approx \phi_{\nu_{\odot}}(p-p) + \phi_{\nu_{\odot}}(^7\text{Be}) + \phi_{\nu_{\odot}}(^8\text{B}). \quad (6)$$

Kamiokande reported

$$\phi_{\nu_{\odot}}(^8\text{B}) = (2.9 \pm 0.4) \times 10^6 \text{ cm}^{-2} \text{ s}^{-1}. \quad (7)$$

Thus, the flux of ^8B neutrinos alone contributes $\langle \sigma \phi \rangle = 3.2 \pm 0.50$ SNU's to the ^{37}Ar production rate in ^{37}Cl , assuming a cross section of $(1.11 \pm 0.03) \times 10^{-42}$ cm 2 for the capture of ^8B neutrinos by ^{37}Cl (Aufderheide et al. 1994). The chlorine experiment at Homestake that is sensitive also to ^7Be neutrinos observed since 1970 an ^{37}Ar production rate of only 2.55 ± 0.25 SNU's, and 2.78 ± 0.35 SNU's in runs 91–124 during 1986–1993, the

running period of Kamiokande II and III. For standard solar neutrinos, these results leave very little room for a ^7Be solar neutrino flux (the SSM estimates its expected contribution at a level of ~ 1 SNU). Therefore, we conclude (Dar 1993) that $\phi_{\nu_{\odot}}(^7\text{Be}) \ll \phi_{\nu_{\text{SSM}}}(^7\text{Be})$ and $\phi_{\nu_{\odot}} \approx \phi_{\nu_{\odot}}(p-p)$. Consequently, the expected ^{71}Ge production rate in ^{71}Ga is given by

$$\langle \sigma \phi_{\nu_{\odot}} \rangle_{\text{Ga}} \approx \langle \sigma \phi_{\nu_{\odot}}(L_{\odot}) \rangle_{\text{Ga}} + \langle \sigma \phi_{\nu_{\odot}}(\text{KAM}) \rangle_{\text{Ga}} = 83 \text{ SNU's}, \quad (8)$$

where the first term on the right-hand-side is the contribution of the $p-p$ solar neutrino flux estimated from the solar luminosity and the second term is the contribution from the ^8B solar neutrino flux measured by Kamiokande. This predicted signal is in excellent agreement with the 79 ± 12 SNU's measured by GALLEX and the 73 ± 19 SNU's measured by SAGE.

Note, however, that in view of the experimental uncertainties, the observed signal in the chlorine experiment is not significantly smaller than the expected minimal signal due to the solar neutrino flux measured by Kamiokande. Thus, the solar neutrino experiments do not provide conclusive evidence for new electroweak physics as claimed, for instance, by Bahcall & Bethe (1993). Although neutrino oscillations, and in particular the MSW effect (Mikheyev & Smirnov 1985; Wolfenstein 1978), can solve the solar neutrino problems, the inferred neutrino mixing parameters seem to differ substantially from those implied by the atmospheric neutrino anomaly (for a recent summary see, e.g., Barish 1995) or those implied by the neutrino anomaly observed by the LSND collaboration at LAMPF (Louis 1995; Athanassopoulos et al. 1995; see, however, Hill 1995). Moreover, in spite of extensive laboratory searches and many precision tests, no confirmed evidence from accelerator experiments has been found for new physics beyond the standard electroweak model (e.g., Langacker 1995, and references therein). Without such evidence, it is quite important to improve the standard solar model (which provides only an approximate description of the complicated Sun) and to continue the search for a standard physics solution to the solar neutrino problems.

In this paper, we present an improved standard solar model and its predictions for the solar neutrino fluxes. The model includes pre-main-sequence evolution, diffusion of all elements, partial ionization effects, and all the significant nuclear reactions between the various elements which the Sun is made of. It uses updated values for the initial solar element abundances, the solar age, the solar luminosity, the nuclear reaction rates, and the radiative opacities. Neither nuclear equilibrium nor complete ionization are assumed. It employs a very fine zoning of the Sun and accurate numerical procedures to integrate the solar evolution equations from zero age until the present day. The calculated solar neutrino fluxes are compared with those measured by the four solar neutrino experiments. The calculated ^8B solar neutrino flux is consistent, within the theoretical and experimental uncertainties, with the solar neutrino observations at Homestake and Kamiokande. However, the observations appear to suggest that the ^7Be solar neutrino flux is much smaller than that predicted by our solar model. In spite of the facts that the value of the ^7Be solar neutrino flux is a robust prediction of the current standard solar models and that minimal extensions of the standard electroweak model,

such as neutrino flavor mixing, can explain its suppression, as will be explained in § 7, we do not consider the ${}^7\text{Be}$ deficit to be compelling evidence for new electroweak physics, as claimed by various authors (e.g., Bahcall & Bethe 1991; Bludman et al. 1993; Castellani et al. 1994; Hata et al. 1994; Berezinsky 1994; Kwong & Rosen 1994; Bahcall 1994; Parke 1995; Hata & Langacker 1995). This is because neutrino absorption cross sections near threshold in ${}^{37}\text{Cl}$ and in ${}^{73}\text{Ga}$ may be significantly smaller than those calculated by Bahcall (1989), because the standard solar models are only approximate and simplified descriptions of the real and complex Sun, and because very little is known, either experimentally or theoretically, about dense plasma effects on nuclear reactions rates, decay rates, and particle and energy transport at solar conditions.

Our paper is organized as follows: In § 2 we outline the standard solar model. In § 3 we describe the astrophysical parameters that we use in this work. The main physics input is described in § 4. Section 5 outlines our stellar evolution code. Our main results are described in § 6 and are compared there with experimental results and the results of other solar model calculations. Possible standard physics solutions to the solar neutrino problem are outlined briefly in § 7. The neutrino mixing parameters suggested by the MSW solution are derived analytically in § 8. Final conclusions are drawn in § 9.

2. THE STANDARD SOLAR MODEL: AN OVERVIEW

The standard solar model (e.g., Bahcall 1989, and references therein) is a physical description of the sun based on *the standard stellar evolution equations* (e.g., Clayton 1968) that are used to calculate its evolution from the premain sequence Hayashi phase to its present state, using *the best available input physics* (initial conditions, equations of state, nuclear cross sections, radiative opacities, condensed matter effects). The model assumes a complete spherical symmetry, no mass loss or mass accretion, no angular momentum gain or loss, no differential rotation, and a zero magnetic field through the entire solar evolution. Thus, the *assumed initial conditions* are as follows:

1. Fully convective, homogeneous, spherically symmetric protostar.
2. Initial mass of $M_{\odot} = 1.99 \times 10^{33}$ g.
3. No angular momentum, no differential rotation, no magnetic field.
4. Initial chemical composition deduced from primitive meteorites, the solar photosphere, the solar wind, the local interstellar gas, and the photospheres of nearby stars.

The calculations are iterated, treating the unknown initial ${}^4\text{He}$ abundance and the mixing length in the convective zone (roughly the size of the pressure scale height) as adjustable parameters, until *the present-day properties of the Sun* are reproduced. These include the following:

1. The solar luminosity $L_{\odot} = 3.844 \times 10^{33}$ ergs s^{-1} .
2. The solar radius $R_{\odot} = 6.9599 \times 10^{10}$ cm.
3. The observed solar surface element abundances.
4. Internal structure consistent with helioseismology data (optional).

The output of the calculations includes the present-day density profile $\rho(r)$, temperature profile $T(r)$, and chemical composition profile $[X_i(r)]$ of the Sun. They can be compared with information extracted from helioseismology.

They can also be used to calculate the expected fluxes of solar neutrinos. In particular, according to the standard model, solar neutrinos are produced mainly in the fusion of hydrogen into deuterium ($p + p \rightarrow \text{D} + e^+ + \nu_e$ and $p + e + p \rightarrow \text{D} + \nu_e$), in electron capture by ${}^7\text{Be}$, and in β decay of ${}^8\text{B}$, ${}^{13}\text{N}$, ${}^{15}\text{O}$, and ${}^{17}\text{F}$. Their production rates in the Sun are calculated using the standard electroweak theory and the density, temperature, and element abundances in the Sun provided by the standard solar model. Our calculations were performed with an updated version of the solar evolution code of Kovetz & Shaviv. We refer the reader to its detailed description by Kovetz & Shaviv (1994) and focus here only on main points and important improvements.

3. THE ASTROPHYSICAL PARAMETERS

3.1. Solar Luminosity

The absolute luminosity of the Sun changes with time due to solar evolution. In addition to this secular solar variability, the solar luminosity changes with solar activity. The solar activity, its period, and erratic disappearance (last time during the Maunder minimum) are not well understood. Precise measurements of the solar “constant” during a large fraction of an entire solar cycle have been carried out on a variety of spacecrafts and satellites during the last two solar cycles (21 and 22). They include the *Nimbus 7* spacecraft (see, e.g., Hickey et al. 1982), the *Solar Maximum Mission* satellite (see, e.g., Wilson & Hudson 1988), the Earth Radiation Budget satellite, the NOAA 9 and NOAA 10 satellites (see, e.g., Lee et al. 1991) and the Upper Atmosphere Research satellite (see, e.g., Wilson 1993). Using the following parameterization of the variation of the solar constant (SC) during the solar cycle (Wilson & Hudson 1988),

$$\text{SC}(t) = S \left[1 + b \left\{ \cos \left[2\pi(t - 1980.82)/10.95 \right] \right\} \right] \text{W m}^{-2}, \quad (9)$$

we found a weighted mean average $S = 1367.2 \pm 3.4$ W m^{-2} for the solar constant. It yields a mean solar luminosity of $L_{\odot} = 4\pi D^2 S = 3.844 \times 10^{33}$ ergs s^{-1} . This value is consistent with the value quoted by the Particle Data Group (1994) and used in BP95. It is smaller by 0.4% than the value $L_{\odot} = 3.86 \times 10^{33}$ ergs s^{-1} used in BP92 and larger by 0.5% than $L_{\odot} = 3.826 \times 10^{33}$ ergs s^{-1} quoted before by the Particle Data Group (1992) and used by Dar & Shaviv (1994).

3.2. Solar Age

The solar age is best estimated from radioactive dating of meteoritic condensation based on the observed ${}^{235}\text{U}/{}^{238}\text{U}$ and ${}^{207}\text{Pb}/{}^{206}\text{Pb}$ ratios. Tilton (1988) estimated this age to be 4.56×10^9 yr. Guenther (1989) estimated it to be 4.49×10^9 yr, while recent analyses by Gopel et al. (1994) and by Wasserburg et al. (1995) yielded $t_{\odot} = (4.566 \pm 0.005) \times 10^9$ yr. This value was used by us as the total solar age which includes both the pre-main-sequence evolution (some $30\text{--}40 \times 10^6$ yr) and the time spent by the Sun on the main sequence.

3.3. Initial Chemical Composition

The initial element abundances influence significantly the solar evolution and the present density, chemical composition, and temperature in the solar core, which determine the solar neutrino fluxes. In particular, the calculated radiative

opacities, which in turn determine the temperature gradient in the solar interior, are very sensitive to the heavy element abundances (the heavy elements are not completely ionized in the Sun). There are four major sources of information on the initial solar abundances. They are the chemical composition of the most primitive class of meteorites (type I carbonaceous chondrites), the solar photospheric abundances, the chemical composition of the solar wind, and the local interstellar medium element abundances.

3.3.1. The Heavy Metal Abundances

Apart from the noble gases, only a few elements, namely, H, C, N, and O, have escaped complete condensation in primitive early solar system meteorites because they were able to form highly volatile molecules or compounds (see, e.g., Sturenburg & Holweger 1990). Thus, the initial solar abundances of all other elements are expected to be approximately equal to those found in type I carbonaceous chondrites as a result of their complete condensation in the early solar system. Since the chemical composition of the solar surface is believed to have changed only slightly during the solar evolution (by nuclear reactions during the Hayashi phase, by diffusion and turbulent mixing in the convective layer during the main-sequence evolution, and by cosmic-ray interactions at the solar surface), it has been expected that the photospheric abundances of these elements are approximately equal to those found in CI chondrites. Over the past decades, there have been many initial disagreements between the meteoritic and photospheric abundances. In nearly all cases, when the atomic data were steadily improved and the more precise measurements were made, the photospheric values approached the meteoritic values. The photospheric abundances are now as a rule in very good agreement with the meteoritic values (Grevesse & Noels 1993a). Hence, as meteoritic values represent the initial values and are known with much better accuracy (often better than 10%) than the photospheric ones, we have assumed that the initial solar heavy metal abundances are given approximately by the meteoritic (CI chondrites) values of Grevesse & Noels (1993a).

3.3.2. The CNO Abundances

The careful and comprehensive analysis of atomic and molecular lines of C, N, and O in the solar photosphere by Lambert (1978) has served as the standard source of their solar abundance. Improved atomic data, non-LTE corrections and study of infrared lines have slightly changed the standard values of the photospheric CNO abundances to those given in Table 1. These values are very much different from those found in primitive meteorites. In particular, carbon and nitrogen are underabundant in CI chondrites by about an order of magnitude compared with their photospheric abundances (e.g., Sturenburg & Holweger 1990; Grevesse et al. 1990). We have assumed in our calculations that the initial CNO abundances are given by the photospheric abundances properly corrected for diffusion during the entire solar evolution.

3.3.3. The Abundances of ^4He and ^3He

Because the Sun is a G2 star, its photospheric helium abundance cannot be measured directly. The photospheric helium abundance of much younger hotter B stars in the solar neighborhood (which are much younger) can be used only for rough estimates of its initial solar abundance. The initial ^4He mass fraction in the solar nebula is known only

TABLE 1

SUMMARY OF INFORMATION ON ABUNDANCES OF VARIOUS ELEMENTS RELATIVE TO HYDROGEN [$A \equiv \log ([A]/[H]) + 12$] IN PRIMITIVE METEORITES, IN THE SOLAR PHOTOSPHERE, IN THE SOLAR WIND, AND IN THE LOCAL INTERSTELLAR MEDIUM, USED IN THE DS STANDARD SOLAR MODELS

Element	Abundance	Source	Reference
D	7.22 ± 0.05	Meteorites, solar wind	1, 2
^3He	7.18 ± 0.08	Meteorites, solar wind	2
^7Li	$1.54 \pm 0.0X$	Meteorites	3
^9Be	$1.13 \pm 0.0X$	Meteorites	3
^{12}C	8.55 ± 0.05	Photosphere	4
^{13}C	6.60 ± 0.05	Photosphere	4
^{14}N	7.97 ± 0.07	Photosphere	4
^{16}O	8.78 ± 0.07	Photosphere	4
^{20}Ne	8.08 ± 0.06	Photosphere	4
^{23}Na	6.33 ± 0.03	Meteorites, photosphere	4
^{24}Mg	7.58 ± 0.05	Meteorites, photosphere	4
^{27}Al	6.47 ± 0.07	Meteorites, photosphere	4
^{28}Si	7.66 ± 0.05	Meteorites, photosphere	4
^{31}P	5.45 ± 0.04	Meteorites, photosphere	4
^{32}S	7.21 ± 0.06	Meteorites, photosphere	4
^{35}Cl	5.5 ± 0.3	Meteorites, photosphere	4
^{40}Ar	6.52 ± 0.1	Meteorites, photosphere	4
^{40}Ca	6.36 ± 0.02	Meteorites, photosphere	4
^{40}K	4.85	Meteorites, photosphere	4
^{45}Sc	3.08	Meteorites, photosphere	4
^{48}Ti	5.02 ± 0.06	Meteorites, photosphere	4
^{50}V	3.99	Meteorites, photosphere	4
^{52}Cr	5.67 ± 0.03	Meteorites, photosphere	4
^{55}Mn	5.39 ± 0.03	Meteorites, photosphere	4
^{56}Fe	7.50 ± 0.04	Meteorites, photosphere	4
^{63}Cu	4.15	Meteorites, photosphere	4
^{58}Ni	6.25 ± 0.04	Meteorites, photosphere	4
^{64}Zn	4.33	Meteorites, photosphere	4
Z/X	0.0245	Meteorites, photosphere	4

REFERENCES.—(1) Linsky et al. 1993. (2) Geiss 1993. (3) Anders & Grevesse 1989. (4) Grevesse & Noels 1993a, 1993b.

approximately, $0.24 < Y < 0.30$. The predictions of the solar models are rather sensitive to the initial mass fraction of ^4He . Consequently, the initial ^4He solar abundance has been treated in the standard solar models as an adjustable parameter. The present-day ^4He surface mass fraction can be inferred from helioseismology data, which yield a surface ^4He mass fraction of $Y_s = 0.242 \pm 0.003$ (Hernandez & Christensen-Dalsgaard 1994). However, their formal error is highly misleading because of the great sensitivity of the result to the model of the solar atmosphere, the equation of state there, and the atmospheric opacities. We estimate that at present the ^4He mass fraction at the solar surface is not known from helioseismology better than $Y_s = 0.242 \pm 0.030$.

From measurement of the $[^3\text{He}]/[^4\text{He}]$ ratio in meteorites and in the solar wind and from the above rough estimate of the initial abundance of ^4He , Geiss (1993) concluded that the presolar abundance of ^3He is $[^3\text{He}]/[\text{H}] = (1.5 \pm 0.3) \times 10^{-5}$ (by numbers), i.e., $\log ([^3\text{He}]/[\text{H}] + 12) = 7.18 \pm 0.08$.

3.3.4. The Deuterium Abundance

Deuterium is easily destroyed already at relatively low temperatures. Consequently, all the primordial deuterium has been destroyed in the Hayashi phase, and its initial abundance cannot be estimated from the solar photosphere. The deuterium abundance in the local interstellar medium was measured recently with the *Hubble Space Telescope* (Linsky et al. 1993) to be $[\text{D}]/[\text{H}] = 1.65_{-0.18}^{+0.07} \times 10^{-5}$ (by numbers), i.e., $\log ([\text{D}]/[\text{H}] + 12) = 7.22 \pm 0.05$. This value

is consistent with the initial solar value, $[D]/[H] = (2.6 \pm 1.0) \times 10^{-5}$, obtained by Geiss (1993) from the analysis of solar wind particles captured in foils exposed on the Moon and from studies of primitive meteorites, which we used.

3.3.5. *The Abundances of ${}^7\text{Li}$, ${}^9\text{Be}$, and ${}^{11}\text{B}$*

The photospheric abundances of ${}^7\text{Li}$, ${}^9\text{Be}$, and ${}^{11}\text{B}$ are smaller by factors of nearly 150, 3, and 10, respectively, than their meteoritic abundances. The origin of such large differences is still not clear. However, the initial solar (meteoritic) abundances of lithium, beryllium, and boron are very small and do not play any significant role in solar evolution. On the other hand, their depletion can provide a clue to the history of the convection zone and the solar evolution.

4. THE PHYSICAL INPUT

4.1. *Nuclear Reaction Rates*

The cross sections for most of the nuclear reactions that play important roles in the Sun fall steeply when the energy drops below the Coulomb barrier. At solar energies, they become too small to be measured directly in laboratory experiments. Consequently, they are either calculated theoretically or extrapolated from laboratory measurements at much higher energies. Because the results of different experiments often differ considerably, and because different theoretical models used for the extrapolation often yield different results, the nuclear reaction rates used in different standard solar models depend on personal judgment. Below we discuss briefly some of the problematics of obtaining reliable thermonuclear reaction rates for solar conditions, and explain our specific choices. These choices are also summarized and compared with the choices of BP95 in Table 2. For all other reactions, we have chosen to use the most detailed and complete compilation of thermonuclear reaction rates published by Caughlan & Fowler (1988).

4.1.1. *The Problematics*

To eliminate from the extrapolation the strong energy dependence due to Coulomb barrier penetration, cross sections are normally parameterized as

$$\sigma_{ij}(E) = \frac{S_{ij}(E)}{E} e^{-2\pi\eta}, \quad (10)$$

where $2\pi\eta = 31.29Z_iZ_j(\mu/E)^{1/2}$ is the Sommerfeld parameter, Z_i and Z_j being the charge numbers of the colliding nuclei, μ their reduced mass in atomic mass units, and E their center-of-mass energy in keV. The factor $S_{ij}(E)$ is expected to vary rather slowly with energy. It is usually

TABLE 2

COMPARISON BETWEEN THE ASTROPHYSICAL S FACTORS FOR THE p - p CHAIN REACTIONS USED IN BP95 AND IN DS94 AND DS95

Reaction	$S^{\text{BP}}(0)$ (keV barns)	$S^{\text{DS}}(0)$ (keV barns)
${}^1\text{H}(p, e^+ \nu_e)\text{D}$	3.896×10^{-22}	4.07×10^{-22}
${}^1\text{H}(pe^- \nu_e)\text{D}$ ^a	... ^b
${}^3\text{He}({}^3\text{He}, 2p)\text{He}^4$	4.99×10^3	5.6×10^3
${}^3\text{He}({}^4\text{He}, \gamma){}^7\text{Be}$	0.524	0.45
${}^7\text{Be}(e^-, \nu_e)\text{Li}^7$ ^a	... ^b
${}^7\text{Be}(p, \gamma){}^8\text{B}$	0.0224	0.017

^a See Bahcall 1989.

^b See Caughlan & Fowler 1988.

extracted from the measured cross section at laboratory energies and extrapolated to the lower solar energies, using either a polynomial fit or an energy dependence that follows from a specific model for the reaction.

The uncertainties in the nuclear reaction rates at solar conditions are still large due to (1) uncertainties in the measured cross sections at laboratory energies, (2) uncertainties in the extrapolations of the $S_{ij}(E)$ from laboratory energies down to solar energies, and (3) uncertainties in dense plasma effects (screening, correlations, and fluctuations) on reaction rates. Unfortunately, only for a few simple reactions ($p + p \rightarrow \text{D} + e^+ + \nu_e$, $p + e + p \rightarrow \text{D} + \nu_e$, and $e^- + {}^7\text{Be} \rightarrow {}^7\text{Li} + \nu_e$), the cross sections can be calculated accurately from theory. For all other direct reactions, neither the microscopic methods (for reviews see, e.g., Langanke 1991) such as the resonating group method (RGM) and the generator coordinate method (GCM), nor the potential models such as the optical model (OM) and the distorted wave Born approximation (DWBA), can predict accurate and reliable low-energy cross sections. For instance, the RGM and the GCM, which are currently considered to be the best theoretical methods for calculating direct nuclear reactions, predict (see, e.g., Descouvemont & Baye 1994; Johnson et al. 1992) $S_{1,7}(0) \approx 25\text{--}30$ eV barns for the reaction $p + {}^7\text{Be} \rightarrow {}^8\text{B} + \gamma$. However, a simple inspection of the results of these models reveals that they reproduce poorly the magnitude of the measured cross section, the position of the resonance, the width of the resonance, the height of the resonance, and the observed shape of the cross section as function of energy. To avoid these discrepancies, only the energy dependence of these models has been used by Johnson et al. (1992) to extrapolate the measured cross sections to $E = 0$, yielding $S_{1,7}(0) \approx 22.4$ eV barns. This value has been used in BP92 and BP95. However, the procedure used by Johnson et al. (1992) is rather an ad hoc one, and it is questionable in view of the facts that (a) their model does not reproduce accurately enough the measured energy dependence of the cross section at lab energies, and (b) they have extrapolated an ‘‘average cross section’’ obtained by averaging cross sections which differ by many standard deviations and have different energy shapes: The cross sections measured by Kavanagh (1960) and by Parker (1968) differ by more than 3σ from the cross sections measured later by Vaughn et al. (1970) and by Filippone et al. (1983) in the same energy ranges [$\text{Kavanagh}/\text{Filippone}] = 1.34 \pm 0.11$, [$\text{Parker}/\text{Vaughn}] = 1.42 \pm 0.13$; see, e.g., Gai 1995).

4.1.2. *The Choice of Extrapolation*

Dar & Shaviv (1994) have pointed out that sub-Coulomb radiative captures and transfer reactions take place mainly when the colliding nuclei are far apart and not when their centers overlap. They argued that most of the energy dependence of the astrophysical $S_{ij}(0)$ factors is because equation (10) ignores this fact. The Coulomb barrier penetration factor $\exp(-2\pi\eta)/(E)^{1/2}$ in equation (10) actually represents

$$|\psi_c(0)|^2 \approx \frac{2\pi\eta}{e^{2\pi\eta} - 1}, \quad (11)$$

the absolute value squared of the Coulomb wave function at the origin (normalized asymptotically to a plane wave of unit amplitude), while the physical cross section is proportional to the square of the Coulomb wave function at the effective distance R at which the reaction takes place,

i.e., to the Coulomb barrier penetration factor at a relative distance R . They concluded that the optical models that describe well the shapes of the bound state and relative motion wave functions outside the nuclear potential are the most reliable for extrapolating the laboratory cross sections to solar energies. Alternatively, they proposed that after extracting the energy dependence of the Coulomb barrier penetration factor to the effective distance R at which the reaction takes place (and other trivial energy dependencies), a simple polynomial fit can be used to extrapolate the lab cross section to solar energies.

Let us show that the reactions take place mainly when the nuclei are far apart. Consider, for instance, radiative captures. The transition amplitude is proportional to an overlap integral $I = \int u^*(r)r\psi_c(r)dr$, where u and ψ_c are the radial parts of the bound state wave function and of the Coulomb distorted wave function of the initial relative motion, respectively. The bound state wave function outside the nuclear radius falls exponentially and has the asymptotic form, $u(r) \sim e^{-\beta r}$, where $\beta = (2\mu E_b)^{1/2}/\hbar$, with E_b being the nuclear binding energy of the colliding nuclei in the final nucleus. The incident Coulomb wave function decreases inside the Coulomb barrier (in the WKB approximation) like

$$\psi_c(r) \sim [V_c(r) - E]^{-1/4} \times \exp \left\{ -\frac{\sqrt{2\mu}}{\hbar} \int_r^{R_0} [V_c(r) - E]^{1/2} dr \right\}, \quad (12)$$

where $V_c(r)$ is the effective Coulomb potential (Coulomb plus centrifugal) and R_0 is the classical turning point. At keV energies, E is much smaller than $V_c(r)$ near the nucleus, and

$$\psi_c(r) \sim r^{+1/4} e^{-2\eta[\pi/2 - \arcsin(E/E_c)^{1/2} - (E/E_c)^{1/2}(1 - E/E_c)^{1/2}]} \sim r^{1/4} e^{\gamma r}, \quad (13)$$

where $E_c = Z_i Z_j e^2/r$ and $\gamma = (8Z_i Z_j e^2 \mu)^{1/2}/\hbar$. Consequently, the contribution to the radial overlap integral comes mainly from the vicinity of $r = R$, where

$$R \approx \frac{\gamma^2}{(4\beta)^2} \left(1 + \sqrt{1 + \frac{20\beta}{\gamma^2}} \right)^2 \approx \frac{\gamma^2}{4\beta^2} = \frac{Z_i Z_j e^2}{E_b}. \quad (14)$$

As an example, for the reaction ${}^3\text{He} + {}^4\text{He} \rightarrow {}^7\text{Be} + \gamma$, one finds $R \approx 10$ fm, while for the reaction $p + {}^7\text{Be} \rightarrow {}^8\text{B} + \gamma$ one finds $R \approx 70$ fm, in good agreement with the optical model and DWBA calculations. Equation (14) is valid only if $R_N \leq R \leq R_0$, where R_N is the nuclear radius of the $i + j$ bound state and $R_0 = Z_i Z_j e^2/E$ is the classical turning point. If $R < R_N$, then $R \approx R_N$. Similarly, if $R \geq R_0$, then $R \approx R_0$. Thus, instead of being proportional to the Coulomb barrier penetration factor at the origin, the radiative capture cross section is proportional to $k_\gamma^3 |u(R)R\psi_c(R)|^2$. One can divide out this energy dependence and use a polynomial fit to extrapolate the reduced cross section to solar energies (Dar & Shaviv 1994) or use instead the optical model or DWBA to extrapolate the total cross section to solar energies. The resulting astrophysical S_{ij} factors are very similar. They are summarized here only for the main reactions.

4.1.3. $S_{17}(0)$

Extrapolations of the cross sections measured by Vaughn et al. (1970) and by Filippone et al. (1983), using either

simple potential models or the above very general properties of sub-Coulomb cross section, gave $S_{17}(0) \approx 17$ eV barns (Barker & Spear 1986; Dar & Shaviv 1994; Kim et al. 1995). This value seems to be supported also by other types of experiments: Analysis of recent measurements of the virtual reaction $\gamma_\nu + {}^8\text{B} \rightarrow p + {}^7\text{Be}$ through Coulomb dissociation of ${}^8\text{B}$ in the Coulomb field of lead (Motobayashi et al. 1994) gave $S_{17}(0) \approx 17$ eV barns. A similar value, $S_{17}(0) \approx 17.6$ eV barns, was estimated from the virtual reaction $p_\nu + {}^7\text{Be} \rightarrow {}^8\text{B}$ measured through the proton transfer reaction ${}^3\text{He} + {}^7\text{Be} \rightarrow \text{D} + {}^8\text{B}$ (Xu et al. 1994). Consequently, we have adopted the value $S_{17} = 17$ eV barns in our standard solar model calculations. The value $S_{17} = 22.4$ eV barns was used in BP92 and BP95.

4.1.4. $S_{34}(0)$

The value $S_{34}(0) = 0.51 \pm 0.02$ keV barns was obtained from measurements of the prompt γ -ray emitted in the reaction ${}^3\text{He} + {}^4\text{He} \rightarrow {}^7\text{Be} + \gamma$, while measurements of the induced ${}^7\text{Be}$ activity led to a weighted average $S_{34}(0) = 0.58 \pm 0.02$ keV barns, which are different by 3.5 standard deviations. The origin of this discrepancy is still not known (Hilgemeier et al. 1988). Normalization to known cross sections favors the lower value.

Using the measured energy dependence of the cross section for ${}^3\text{He} + {}^4\text{He} \rightarrow {}^7\text{Be} + \gamma$ by Krawinkel et al. (1982) for extrapolating the cross sections measured by prompt gamma-ray emission (Parker & Kavanagh 1963; Osborne et al. 1984; Krawinkel et al. 1982 [multiplied by 1.4]; Hilgemeier et al. 1988) to zero energy, we obtained $S_{34}(0) = 0.45$ keV barns. The value $S_{34}(0) = 0.533$ keV barns was used in BP92, and $S_{34}(0) = 0.524$ keV barns was used in BP95.

4.1.5. $S_{33}(0)$

A similar analysis of the low-energy data of Greife et al. (1994), Krauss et al. (1987), and Dawarakanath & Winkler (1971) on the reaction ${}^3\text{He} + {}^3\text{He} \rightarrow {}^4\text{He} + 2p$ gave $S_{33}(0) = 5.6$ MeV barns. Essentially the same value, $S_{33}(0) = 5.57$ MeV barns, was obtained by Krauss et al. (1987) and by Greife et al. (1994) by applying a polynomial fit to their data. The value $S_{33}(0) = 5.0$ MeV barns was used in BP92, and $S_{33}(0) = 4.99$ MeV barns was used in BP95.

4.1.6. $S_{11}(0)$

The cross section for the reaction $p + p \rightarrow \text{D} + e^+ + \nu_e$ is too small to be measured directly in the laboratory. The measured cross sections for the weak isospin related reactions $\bar{\nu}_e + \text{D} \rightarrow e^+ + n + n$, $\bar{\nu}_e + \text{D} \rightarrow \bar{\nu}_e + p + n$, and $\gamma + \text{D} \rightarrow n + p$ (Suzuki et al. 1995) were used to obtain the relevant nuclear matrix element needed for calculating the cross section for $p + p \rightarrow \text{D} + e^+ + \nu_e$. This procedure yielded a best value $S_{11}(0) \approx 0.47 \times 10^{-22}$ keV barns, which is consistent with the value used by Caughlan & Fowler (1988). It is 4.2% larger than the value $S_{11}(0) \approx 3.896 \times 10^{-22}$ keV barns calculated recently by Kamionkowski & Bahcall (1994) and used in BP95.

Table 2 compares the astrophysical $S_{ij}(0)$ factors used in this work (and also in DS94) and in BP95.

4.2. Screening Enhancement of Reaction Rates

Screening of target nuclei by their electrons is known to enhance significantly laboratory nuclear cross sections at very low energies (e.g., Engstler et al. 1988), although a complete theoretical understanding of the effect is still

lacking (see, e.g., Shoppa et al. 1993, Rolfs 1994, and references therein). Screening corrections to the nuclear reaction rates in the SSM are usually represented by an enhancement factor

$$F \approx e^{\Delta U/kT} \approx e^{Z_i Z_j^2 e / R_D kT}, \quad (15)$$

where ΔU is the gain in electronic potential energy when an incident ion of charge $Z_j e$ penetrates the charged cloud around an ion of charge $Z_i e$, T is the plasma temperature, and R_D is the Debye length, $R_D \equiv (kT/4\pi e^2 \Sigma Z^2 \bar{n}_z)^{1/2}$. This screening enhancement of thermonuclear reaction rates near the center of the Sun is quite considerable, being 5%, for the p - p and pep -reactions, 20% for the ${}^3\text{He}{}^3\text{He}$, ${}^3\text{He}{}^4\text{He}$, and $p{}^7\text{Be}$ reactions, and 30%, 35%, and 40% for the p capture by the C, N, and O isotopes, respectively.

The change in the Coulomb barrier (or equivalently the gain in energy) due to screening is estimated from the Debye-Hückel (DH) approximation for the screened potential around a static ion in an electrically neutral plasma ($\Sigma Z \bar{n}_z = 0$, \bar{n}_z being the number density of particles of charge Ze with $Z = -1$ for electrons):

$$\Phi_i = \frac{eZ_i}{r} e^{-r/R_D} \approx \frac{eZ_i}{r} - \frac{eZ_i}{R_D} \quad \text{for } r \ll R_D, \quad (16)$$

which is an approximate solution to Poisson's equation

$$\nabla^2 \Phi_i = 4\pi e \Sigma Z n_z = 4\pi e \Sigma Z \bar{n}_z e^{-eZ\Phi_i/kT} \approx R_D^2 \Phi_i, \quad (17)$$

near a static ion of charge Z_i . This equation and solution, however, are valid only far from the nucleus where $eZ\Phi_i \ll kT$, or else the explanation is not valid. In the core of the Sun at which kT (~ 1 keV) is much smaller than the Coulomb barriers (~ 1 MeV) between the reacting nuclei, most of the contribution to the nuclear reaction rates comes from collisions with center-of-mass energies $E \gg kT$. At the classical turning point $eZ_j \Phi_i = E$. Consequently, inside the barrier, $eZ_j \Phi_i \gg kT$, and the naive use of the DH approximate potential for calculating the barrier penetration factor (e.g., Clayton 1968) is unjustified for projectiles with wavelengths much shorter than the classical distance of closest approach. The DH solution assumes also that there are many ions and many electrons within a Debye sphere. Also, these conditions are not quite satisfied in the core of the Sun, where the interior distance is about the same as the Debye length. It was found that when the conditions for the validity of the DH approximation are violated in laboratory plasmas, calculations based on the DH approximation fail dramatically (Goldsmith et al. 1984) in reproducing various observations, unless the wavelength of the particle under consideration is much larger than the Debye length. The latter is the case for the electron capture reaction ${}^7\text{Be}(e^-, \nu_e){}^7\text{Li}$, where it was found by Johnson et al. (1992) that the DH screening potential changes $|\psi_e(0)|^2$ by only a few percent. However, for the thermonuclear reactions in the Sun, the wavelengths of the reacting ions are very small in comparison with their classical distances of closest approach and the Debye length.

Moreover, an ion approaching from infinity a target nucleus gains from the Debye cloud a potential energy $\Delta U \approx e^2 Z_i Z_j / R_D$ when it penetrates it. But there is no gain in potential energy if either its initial position is already inside the Debye cloud (where the cloud potential is constant $V \approx eZ_i / R_D$) or if the ion leaves and enters similar potential wells.

Near the center of the Sun, where $\rho_c \approx 156 \text{ g cm}^{-3}$, $T_c \approx 1.57 \times 10^7 \text{ K}$, $X_c(\text{H}) \approx 34\%$, and $X_c(\text{He}) \approx 64\%$, the average interionic spacing is $\bar{n}_i^{-1/3} \sim 2.8 \times 10^{-9} \text{ cm}$, similar to the Debye length, $R_D \approx 2.3 \times 10^{-9} \text{ cm}$. On the other hand, the gain in potential energy is increased if both ions retain their Debye clouds during their approach. However, the most effective ion energies are $5\text{--}20 kT$, and their velocities are not much smaller than the average thermal electron velocities. There may not be sufficient time for the plasma to rearrange itself around the fast-moving ions and screen them effectively [the typical rearrangement time, $2\pi/\omega_p$, where $\omega_p = (4\pi n_e^2/m_e)^{1/2}$, is longer than the time it takes a fast ion to cross the Debye length]. All these effects may modify substantially the screening enhancement of the fusion reaction rates near the center of the Sun as calculated from the static DH screening potential. Actually, the situation is too complicated for reliable analytic estimates. Reliable estimates, however, may be based on numerical N -body simulation of the classical trajectories of electrons and ions in a dense plasma that can be used to evaluate the various effects of correlations and fluctuations on the thermonuclear reaction rates in dense plasmas (Shaviv & Shaviv 1996). To test the sensitivity of the standard solar models to the screening corrections, we have carried out the calculations with and without the standard screening enhancement factors of all the thermonuclear reaction rates. We found (Dar & Shaviv 1994) that removing/including the screening enhancement factors for *all* nuclear reaction rates had only a small effect on the calculated solar neutrino fluxes, due to accidental cancellations. Screening enhancement may, however, play important roles in other stars. Moreover, changes in the screening factors that change their ratios for the different reactions may cause significant changes in the calculated solar neutrino fluxes.

4.3. Radiative Opacities

The radiative opacities depend on the local chemical composition, density, and temperature in the Sun. We have used radiative opacity tables computed by the OPAL group at Lawrence Livermore National Laboratory that were kindly provided to us by F. J. Rogers. They are updated version of the OPAL tables of Rogers & Iglesias (1992) for the most recent determination by Grevesse & Noels (1993a) of the heavy element composition of the Sun from the meteoritic and photospheric data. As for the low-temperature opacities, we used the Alexander, Rympa, & Johnson (1983) low temperature opacities which include the effect of molecules. Note that the original table contains a numerical error. This error was corrected by interpolation from adjacent values. Since the opacities are differentiated for the numerical scheme, a spline interpolation is used to guarantee regular derivatives and opacities. Note that the nuclear reactions and the element diffusion change the heavy element abundance throughout the Sun as well as its internal breakdown to the various elements. The breakdown of the OPAL opacities to the individual contributions of the various elements as function of local density, temperature, and composition is not available yet for general use. However, the calculations of Kovetz & Shaviv (1994) show that the diffusion of the heavy elements is approximately the same for all the heavy metals, including the partial ionization of each element (see, e.g., Table 1 of Kovetz & Shaviv 1994). Thus, the error introduced in the radiative opacity by the neglect of the change in the heavy

element breakdown is expected to be negligible compared to other inaccuracies in the opacities. Besides diffusion, the only important process that changes the relative abundances of the heavy elements is the conversion of ^{12}C to ^{14}N in the core of the Sun. However, since the radiative opacities of C and N are not very different when they are completely ionized, we do not expect this conversion to affect significantly the total radiative opacity. Consequently, we calculated the opacities for the values of ρ , T , X , and Z in each shell by interpolating the OPAL opacities, assuming the same breakdown of Z to the heavy elements. We plan to extend the present calculations to include the effects of the variations of the heavy element breakdown on the radiative opacity.

4.4. Equation of State and Partial Ionization

Under the conditions prevailing in the core of the Sun, the electrons are partially degenerate. Their contributions to the various thermodynamic quantities (pressure, entropy, adiabatic exponents) is calculated in the Kovetz & Shaviv code by exact evaluation of the Fermi-Dirac integrals. The Coulomb interactions in the solar plasma have been included in the nonideal part of the free energy. The value of the Coulomb parameter in the core of the Sun is about 0.1–0.2. Kovetz & Shaviv (1994) and Dar & Shaviv (1994) used a fit by Iben, Fujimoto, & MacDonald (1992) to the results of Slattery, Doolen, & De Witt (1980) for the internal energy of the gas which were obtained for the Coulomb parameter $\Gamma \leq 1$. These results were calculated for a one-component plasma (OCP) and ignore the contribution of the electrons. Recent results by Shaviv & Shaviv (1996) indicate that the assumption of OCP is not so good for such low values of Γ and, hence, we calculated a model with the simple Debye-Hückel model. The local ionization state of each element is calculated by solving the local Saha equations. Partial ionization effects are included in the equation of state and in the diffusion coefficients (C, N, O, or Mg are once to twice ionized at the surface and completely ionized in the core. Fe is doubly ionized at the surface but only 16–20 times ionized in the core). Partial ionization has an important effect on the equation of state in the outer part of the Sun even if the relevant region is convective, since the partial ionization affects the entropy of the gas.

5. THE SOLAR EVOLUTION CODE

Modeling the solar evolution requires integration of the standard stellar evolution equations over very long times. Truncations and inaccuracies in the time integration may add to large errors if not handled properly. In particular, the numerical integration must ensure energy conservation. Namely, the integral of the total solar luminosity in photons and neutrinos over a long time must be equal to the change in the total solar binding energy (nuclear, gravitational, thermal, and Coulomb) during that time. A carefully constructed advanced stellar evolution code was described by Kovetz & Shaviv (1994). We have used this code to calculate the evolution of a $1 M_{\odot}$ protostar, fully convective with a uniform composition, initial solar element abundances and a luminosity around $12 L_{\odot}$. The code follows the Hayashi track, the settling to the main sequence (ZAMS) and the main-sequence evolution. It includes gravitational and nuclear energy release, radiative energy transport, convection, and diffusion of all elements more abundant than a

prescribed abundance. Neither nuclear equilibrium nor complete ionization are imposed. The effects of partial ionization are included in the equation of state, the diffusion coefficients, and the radiative opacities of OPAL and in the calculation of the solar atmosphere. For the convenience of the reader, we highlight here some important details of the stellar evolution code. For more details, the reader is referred to its description in the original paper of Kovetz & Shaviv (1994).

5.1. Nuclear Evolution

The nuclear evolution equations for the local number fractions $y_i = X_i/A_i$ have the general form

$$\frac{dy_i}{dt} = \sum_k S_{i,k}(y)y_k, \quad (18)$$

where $S(y)$ is a matrix with positive (creation) and negative (destruction) elements. Most of these elements are linear in the y 's, but some (corresponding to beta decays) are constants. Thus, the right-hand side of equation (18) is quadratic in the y 's. The basic nuclear network contains all the isotopes and nuclear reactions that appear in Caughlan & Fowler (1988). The nuclear reactions rates have been updated with the reaction rates of Wiescher et al. (1989), Kubono et al. (1989), and Gorres, Wiescher, & Rolf (1989). The other changes (updating the normalization of the $^3\text{He}^3\text{He}$, $^3\text{He}^4\text{He}$, $p^7\text{Be}$ reactions) were described in § 4. The equation is solved by conversion into a finite-difference equation. Stability and the requirement that the solution approaches the solution for nuclear equilibrium as time tends to infinity require that the time differencing be implicit. Thus, equation (18) is replaced by the fully implicit finite-difference system,

$$y_{t+\delta t} = y_t + \delta t S(y_{t+\delta t}) y_{t+\delta t}, \quad (19)$$

which is correct to $O(\delta t)$, is numerically stable, and delivers the correct values $y_i(t + \delta t)$ for those isotopes that change very rapidly and are thus in nuclear equilibrium. No special provision is required for handling isotopes that are in or tend toward nuclear equilibrium. The nonlinear equations (19) are solved by iterations in which large matrices are inverted (which consume a lot of CPU time). About three iterations were needed to obtain an accuracy of $1:10^{-10}$ needed in order to follow the concentration of species like ^7Li and ^8B . Our nuclear network contains about 80 isotopes, of which only the following 18 isotopes were found to play important role in the nuclear evolution: ^1H , ^2D , ^3He , ^4He , ^7Li , ^9Be , ^8B , ^{12}C , ^{13}C , ^{13}N , ^{14}N , ^{15}N , ^{15}O , ^{16}O , ^{17}O , ^{17}F , ^{18}F , ^{20}Ne , and ^{23}Na . The nuclear network searches automatically for the most important contributing reactions at each phase. In the particular case of the Sun, the network was reduced to these 18 isotopes. Yet, reactions like ^3HeD were included by the program. (The other elements, in particular Ne, Na, Mg, Si, S, and Fe, which are present in the Sun in significant quantities that affect the “heavy element” abundance Z but do not participate in the nuclear reactions, were included in the calculations of the opacities, the equation of state, the thermodynamic quantities, and the diffusion of elements.) The nuclear energy generation rate Q_N , which is the time derivative of the total nuclear binding energy is calculated from

$$Q_N = -E_b \dot{S}(y_{t+\delta t}) y_{t+\delta t}, \quad (20)$$

where E_b is the vector of nuclear binding energies. This form ensures that the integral over time of the nuclear energy released in the Sun is equal to the change in the solar nuclear binding energy during that time.

5.2. Space and Time Steps

The Sun was divided into 550 mass shells, distributed in such a way to yield sufficiently fine distribution in the core, near the bottom of the outer convective zone (where Δm was $1 \times 10^{-4} M_\odot$) and at the surface. The time steps were constrained in such a way that the changes in $\log T$, $\log \rho$, and $\log X_i$ during a time step were smaller than 0.02, 0.05, and 0.02, respectively. No time steps larger than 3×10^6 yr were allowed. The implicit difference equations, replacing the laws of energy and momentum conservation, were iterated until $\log T$ and $\log \rho$ were determined within 1×10^{-7} .

5.3. Convection

A region in which $d\rho/dp < 0$, or, in the case of uniform composition and ionization, a region in which the entropy decreased outward, was considered to be convective. In a convective region, a complete and instantaneous mixing was carried out, and a convective flux was added to the radiation flux. The convective flux was calculated according to the mixing-length recipe, using the numerical constant of Mihalas (1978, p. 188).

5.4. The Surface Boundary Condition

The outer half of the last mass shell was treated as a static atmosphere. The Stefan-Boltzmann luminosity from the last shell was equated to the total heat flow into the shell, and the effective temperature was adjusted (by iterations) until the calculated entropy (as given by the model atmosphere) at the base of the atmosphere was equal to the entropy (as given by the evolution program) at the center of the shell. The Burlish-Stoer extrapolation method (Press et al. 1989, p. 563) was used for the inward integration. A fine grid of model stellar atmospheres is constructed, and the conditions at the middle of the last mesh point are found by interpolation inside the grid. The model atmosphere starts with the photosphere $\tau = \frac{2}{3}$ and no $T - \tau$ relation is required. The equations of the gray atmosphere are integrated down to the mass of the prescribed (half) last mass shell.

5.5. Diffusion

Diffusion, caused by density, temperature, pressure, chemical composition, and gravitational potential gradients, may play an important role in the Sun. The effects of helium diffusion on solar models were studied first by Noerdlinger (1977). Improved calculations were done by Cox, Guzik, & Kidman (1989), Proffitt & Michaud (1991), and BP92, who incorporated the approximate analytical description of hydrogen and helium diffusion by Bahcall & Loeb (1990) in their standard solar model calculations. Proffitt (1994) and Kovetz & Shaviv (1994) have studied the effects of diffusion on the Sun by solving numerically the diffusion equations for all the elements with mass fraction greater than a prescribed value (usually 10^{-5}). To simplify the numerical handling of the ionization, each isotope was assumed to be in a single ionization stage at each point, the one which is the most abundant. Consequently, the ionization stage changed from one shell to the other, but in each

shell only one state was allowed. The Kovetz-Shaviv code calculates the diffusion of all the individual elements from the pre-main-sequence phase to the present age. The binary and thermal diffusion coefficients depend on the squared ionic charges. The ionization state of each element in every shell is calculated by solving the Saha equations for all the elements in each shell. All elements with mass fractions less than 10^{-5} are treated as trace elements. By trace element, we mean that collisions with other trace elements are neglected. As a consequence of diffusion, the surface and internal element abundances change for each element in a slightly different way. Diffusion depletes the surface abundances of ^4He and the heavy elements. For C, N, and O, only their present photospheric abundances are known (see § 3.3.2). Consequently, in our solar model calculations their initial solar abundances were adjusted to reproduce their observed photospheric abundances. Thus, their initial abundances should be considered as a prediction of the standard solar model. For all other elements, the initial meteoritic abundances are used to predict their final surface abundances, which can be compared with their observed photospheric abundances. The unknown initial abundance of ^4He is treated as a free parameter. It is adjusted to best reproduce the presently observed Sun. Its predicted surface abundance today can be compared with the value derived from helioseismology (Hernandez & Christensen-Dalsgaard 1994).

6. RESULTS AND COMPARISON WITH OBSERVATIONS

Our predictions of the solar neutrino fluxes for three standard solar models are summarized in Table 3A and are compared with the results from the four solar neutrino experiments. The models were calculated with the stellar evolution code of Kovetz & Shaviv (1994) as described in § 5, with the improved astrophysical and physical input data which were described in §§ 3 and 4. The three models differ only in their treatment of element diffusion and equation of state: The model labeled "DSND" does not include element diffusion. The models labeled "DS94" and "DS95" include element diffusion, while model DS95 includes an improved equation of state for $\Gamma \leq 1$. Model DS94 assumes that the initial heavy metal abundances in the Sun were equal to their meteoritic values, and those of C, N, and O were equal to their observed photospheric abundances, as summarized in Table 1. In model DS95 the initial abundances of C, N, and O were adjusted to yield their present-day photospheric abundances, while the heavy metal abundances were assumed to be those found in primitive meteorites, as summarized in Table 1. Table 3B presents some physical characteristics of the three models. The indexes have the following meanings: "c" means the core, "s" means the surface, and 0 means the initial values. R_{conv} is the radius of the base of the convective envelope, and T_{bc} is the temperature at the base of the convective envelope. As can be seen from Table 3A, all three models yield a ^8B solar neutrino flux consistent with that measured by Kamio-kande. However, all three models predict capture rates in the chlorine and gallium experiments that are significantly larger than those measured by Homestake, GALLEX, and SAGE (we have used the neutrino cross sections from Table 8.2 of Bahcall 1989 to convert solar neutrino fluxes to capture rates). Table 4 presents a comparison between four solar models. The model labeled "BP92" is the best model of BP92. It includes diffusion of protons and ^4He but not of

TABLE 3A
COMPARISON OF PREDICTED AND OBSERVED SOLAR NEUTRINO FLUXES^a

ν Flux	DSND	DS94	DS95	Observed	Experiment
$\phi_{\nu}(p-p)$ ($10^{10} \text{ cm}^{-2} \text{ s}^{-1}$).....	6.11	6.06	6.10
$\phi_{\nu}(pep)$ ($10^8 \text{ cm}^{-2} \text{ s}^{-1}$).....	1.43	1.42	1.43
$\phi_{\nu}(^7\text{Be})$ ($10^9 \text{ cm}^{-2} \text{ s}^{-1}$).....	3.57	4.00	3.71
$\phi_{\nu}(^8\text{B})$ ($10^6 \text{ cm}^{-2} \text{ s}^{-1}$).....	2.26	2.60	2.49	2.9 ± 0.4	Kamiokande
$\phi_{\nu}(^{13}\text{N})$ ($10^8 \text{ cm}^{-2} \text{ s}^{-1}$).....	3.10	3.30	3.82
$\phi_{\nu}(^{15}\text{O})$ ($10^8 \text{ cm}^{-2} \text{ s}^{-1}$).....	3.06	3.19	3.74
$\phi_{\nu}(^{17}\text{F})$ ($10^6 \text{ cm}^{-2} \text{ s}^{-1}$).....	3.62	3.84	4.53
$\Sigma(\phi\sigma)_{\text{Cl}}$ (SNU).....	4.2 ± 1.2	4.2 ± 1.2	4.1 ± 1.2	2.55 ± 0.25	Homestake
$\Sigma(\phi\sigma)_{\text{Ga}}$ (SNU).....	116 ± 6	116 ± 6	115 ± 6	79 ± 12	GALLEX
$\Sigma(\phi\sigma)_{\text{Ga}}$ (SNU).....	116 ± 6	116 ± 6	115 ± 6	74 ± 16	SAGE

^a Comparison between solar neutrino fluxes predicted by the current best standard solar models of Dar and Shaviv, with and without element diffusion, and the solar neutrino observations.

TABLE 3B
CHARACTERISTICS OF THE DS SOLAR MODELS IN TABLE 3A

Parameter	DSND	DS94	DS95
$T_c(10^7 \text{ K})$	1.553	1.554	1.561
$\rho_c(\text{g cm}^{-3})$	154.9	155.3	155.4
X_c	0.3491	0.3462	0.3424
Y_c	0.6333	0.6359	0.6380
Z_c	0.01757	0.01802	0.01950
X_s	0.6978	0.7243	0.7512
Y_s	0.2850	0.2597	0.2308
Z_s	0.01703	0.01574	0.0170
$\bar{N}_s(^{12}\text{C})$	8.55	8.50	8.55
$\bar{N}_s(^{14}\text{N})$	7.97	7.92	7.97
$\bar{N}_s(^{16}\text{O})$	8.87	8.82	8.87
$\bar{N}_s(^{20}\text{Ne})$	8.08	8.03	8.08
$\bar{X}(\geq ^{24}\text{Mg})/Z_s$	0.00464	0.00414	0.00415
$R_{\text{conv}}(R/R_{\odot})$	0.7306	0.7105	0.7301
$T_{\text{bc}}(10^6 \text{ K})$	1.97	2.10	2.105
$T_{\text{eff}}(\text{K})$	5895	5920	5803
X_0	0.69775	0.69859	0.7295
Y_0	0.285007	0.28267	0.2509
Z_0	0.01703	0.01931	0.01833

NOTE.—c = center; s = surface; bc = base of convective zone;
 $N = \log([N]/[H] + 12)$.

other elements. The model labeled “BP95” is the best model of BP95 which includes also diffusion of the heavy metals but assumes that all the heavy elements diffuse like fully ionized iron. The predictions of the DS models differ significantly from the BP models because they differ in input physics, approximations, and numerical methods. Most of the differences are due to the use of different reaction rates as summarized in Table 2, the different treatments of diffusion and the equation of state. This is demonstrated in Table 5, where we present a comparison between the best model of BP95 without diffusion labeled BP95ND, and a solar model, labeled DS(BPND), calculated with the Kovetz-Shaviv stellar evolution code with the same physical and astrophysical input parameters and the same nuclear reaction rates used in BP95ND and without inclusion of element diffusion. As can be seen from Tables 5A and 5B, the two calculations yield similar results. Even the fluxes of ^8B and CNO solar neutrinos which, under the imposed solar boundary conditions, are very sensitive to the central solar temperature, differ by less than 4%. These remaining differences are mainly due to the use of different

equations of state, numerical methods, fine zoning and time steps in the two codes, and the inclusion of pre-main-sequence evolution in our code. To emphasize the important role that might be played by diffusion, Tables 5A and 5B also include the current best solar models of Dar & Shaviv (1994) and of Bahcall & Pinsonneault (1995), which include diffusion of all elements. As can be seen from Tables 5A–5B, Bahcall & Pinsonneault (1995) found rather large increases in their predicted ^7Be , ^8B , ^{13}N , ^{15}O , and ^{17}F solar neutrino fluxes; 14%, 36%, 52%, 58%, and 61%, respectively, compared with their model (BP95ND) with no diffusion. These induce 36%, 33%, and 9% increases in the predicted rates in Kamiokande, Homestake, and in GALLEX and SAGE, respectively. However, we predict more moderate increases due to diffusion, 4%, 10%, 23%, 24%, and 25%, respectively, in the above fluxes, which correspond to 10%, 10%, and 2% increases in the predicted rates in Kamiokande, Homestake, and in GALLEX and SAGE, respectively. The differences in the effects of diffusion in DS94 and BP95 are due mainly to two reasons: (a) In the calculations of BP95, all heavy elements were

TABLE 4A
COMPARISON BETWEEN SOLAR NEUTRINO FLUXES PREDICTED BY THE DAR-SHAVIV MODELS AND THE BAHCALL-PINSONNEAULT BEST SOLAR MODELS

Parameter	BP92	DS94	BP95	DS95
$\phi_{\nu}(p-p)$ ($10^{10} \text{ cm}^{-2} \text{ s}^{-1}$).....	6.00	6.06	5.91	6.10
$\phi_{\nu}(pep)$ ($10^8 \text{ cm}^{-2} \text{ s}^{-1}$)	1.43	1.42	1.40	1.43
$\phi_{\nu}(^7\text{Be})$ ($10^9 \text{ cm}^{-2} \text{ s}^{-1}$)	4.89	4.00	5.15	3.71
$\phi_{\nu}(^8\text{B})$ ($10^6 \text{ cm}^{-2} \text{ s}^{-1}$)	5.59	2.60	6.62	2.49
$\phi_{\nu}(^{13}\text{N})$ ($10^8 \text{ cm}^{-2} \text{ s}^{-1}$).....	4.92	3.30	6.18	3.82
$\phi_{\nu}(^{15}\text{O})$ ($10^8 \text{ cm}^{-2} \text{ s}^{-1}$).....	4.26	3.19	5.45	3.74
$\phi_{\nu}(^{17}\text{F})$ ($10^6 \text{ cm}^{-2} \text{ s}^{-1}$)	5.39	3.84	6.48	4.53
$\Sigma(\phi\sigma)_{\text{Cl}}$ (SNU)	8 ± 1	4.2 ± 1.2	9.3 ± 1.4	4.1 ± 1.2
$\Sigma(\phi\sigma)_{\text{Ga}}$ (SNU).....	132 ± 7	116 ± 6	137 ± 8	115 ± 6

TABLE 4B
CHARACTERISTICS OF THE BP95, DS94, AND DS95 SOLAR MODELS IN TABLE 3A

Parameter	BP95	DS94	DS95
T_c (10^7 K)	1.584	1.554	1.561
ρ_c (g cm^{-3}).....	156.2	155.3	155.4
X_c	0.3333	0.3462	0.3424
Y_c	0.6456	0.6359	0.6380
Z_c	0.0211	0.01950	0.01940
X_s	0.7351	0.7243	0.7512
Y_s	0.2470	0.2597	0.2308
Z_s	0.01798	0.01574	0.0170
$\bar{N}_s(^{12}\text{C})$	8.55	8.50	8.55
$\bar{N}_s(^{14}\text{N})$	7.97	7.92	7.97
$\bar{N}_s(^{16}\text{O})$	8.87	8.82	8.87
$\bar{N}_s(^{20}\text{Ne})$	8.08	8.03	8.08
$\bar{X}(\geq ^{24}\text{Mg})/\bar{Z}_s$	0.00414	0.00415
$R_{\text{conv}}(R/R_{\odot})$	0.712	0.7105	0.7301
T_{bc} (10^6 K)	2.20	2.10	2.105
T_{eff} (K)	5920	5803

NOTE.—c = center; s = surface; bc = base of convective zone; $N = \log([N]/[H]) + 12$.

assumed to diffuse at the same rate as fully ionized iron, while the DS95 calculations followed the diffusion of all the elements separately and used diffusion coefficients for the actual ionization state of each element. (b) Bahcall & Pinsonneault assumed that the meteoritic abundances represent the solar surface abundances today and not their initial values. They adjusted their initial values to reproduce

surface abundances today equal to the meteoritic values. Thus, they have actually used an initial ratio $Z/X = 0.0285$ (see Table 4 of BP95), while the observed ratio in meteorites is $Z/X = 0.0245$ (Grevesse & Noels 1993a, 1993b). Dar & Shaviv (1994) and Shaviv (1996) used the meteoritic values for the initial metallic abundances and predicted present-day depleted surface abundances. Unfortunately, the

TABLE 5
SOLAR NEUTRINO FLUX COMPARISON*

Parameter	BP95(ND)	DS(BPND)	BP95	DS95
$\phi_{\nu}(p-p)$ ($10^{10} \text{ cm}^{-2} \text{ s}^{-1}$).....	6.01	6.08	5.91	6.10
$\phi_{\nu}(pep)$ ($10^8 \text{ cm}^{-2} \text{ s}^{-1}$)	1.44	1.43	1.40	1.43
$\phi_{\nu}(^7\text{Be})$ ($10^9 \text{ cm}^{-2} \text{ s}^{-1}$)	4.53	4.79	5.15	3.71
$\phi_{\nu}(^8\text{B})$ ($10^6 \text{ cm}^{-2} \text{ s}^{-1}$)	4.85	5.07	6.62	2.49
$\phi_{\nu}(^{13}\text{N})$ ($10^8 \text{ cm}^{-2} \text{ s}^{-1}$).....	4.07	4.05	6.18	3.82
$\phi_{\nu}(^{15}\text{O})$ ($10^8 \text{ cm}^{-2} \text{ s}^{-1}$).....	3.45	3.38	5.45	3.74
$\phi_{\nu}(^{17}\text{F})$ ($10^6 \text{ cm}^{-2} \text{ s}^{-1}$)	4.02	4.06	6.48	4.53
$\Sigma(\phi\sigma)_{\text{Cl}}$ (SNU)	7 ± 1	7 ± 1	9.3 ± 1.4	4.1 ± 1.2
$\Sigma(\phi\sigma)_{\text{Ga}}$ (SNU).....	127 ± 6	128 ± 7	137 ± 8	115 ± 6

* Comparison between solar neutrino fluxes calculated from the best standard solar model with no diffusion of BP95 and those calculated with the Dar-Shaviv SSM code with the same nuclear reaction rates, opacities, composition, and astrophysical parameters. The predictions of the current best standard solar models of Dar & Shaviv and of Bahcall & Pinsonneault are also included.

uncertainties in the measured photospheric CNO abundances (typically 30%–40%) are much larger than their predicted depletion (typically 10%) and do not allow a reliable test of this prediction.

The photospheric abundances of ${}^7\text{Li}$, ${}^9\text{Be}$, and B are much smaller than their abundances in primitive meteorites. For instance, the photospheric abundance of ${}^7\text{Li}$ is smaller by nearly a factor of 150 (Anders & Grevesse 1989). These differences are not explained by the standard solar models, in spite of the fact that significant lithium burning takes place during the Hayashi phase. However, observations of ${}^7\text{Li}$ in young solar mass stars (e.g., Söderblom et al. 1994) and solar evolution calculations (e.g., Kovetz & Shaviv 1994) suggest that pre-main-sequence destruction of ${}^7\text{Li}$ together with its main-sequence destruction is less than a factor 5 and cannot explain a surface depletion of ${}^7\text{Li}$ by nearly a factor 150. Its destruction (via ${}^7\text{Li} + p \rightarrow {}^4\text{He} + {}^4\text{He}$) requires higher temperatures than about 2.2×10^6 K predicted by the standard solar models for the bottom of the convective zone. Differential rotation below the base of the convective zone may cause mixing and bring ${}^7\text{Li}$ much deeper, where it can burn (see, e.g., Vauclair & Charbonnel 1995). Such mixing may, however, inhibit the inward diffusion of the heavy elements. Thus, it is not clear whether solar models with diffusion (such as DS95) provide a more realistic description of the sun than solar models without diffusion (such as DSND). Helioseismology data, however, are better explained by SSMs with diffusion; see, e.g., Christensen-Dalsgaard et al. (1993).

7. WHERE ARE THE ${}^7\text{Be}$ NEUTRINOS?

As we have seen in § 6, standard solar models predict capture rates in the chlorine and gallium experiments that are significantly larger than those measured by Homestake, GALLEX, and SAGE. Combined with the results from Kamiokande, they seem to suggest that the ${}^7\text{Be}$ solar neutrino flux is strongly suppressed (and perhaps also the fluxes of ${}^8\text{B}$ and CNO solar neutrinos). Can standard physics explain the suppression of the ${}^7\text{Be}$ solar neutrino signal in ${}^{37}\text{Cl}$ and ${}^{71}\text{Ga}$? We think that such a possibility has not been ruled out yet: Electron capture by ${}^7\text{Be}$ into the ground state of ${}^7\text{Li}$ produces 862 keV neutrinos. The threshold energy for neutrino absorption by ${}^{37}\text{Cl}$ is 814 keV. Thus, absorption of ${}^7\text{Be}$ neutrinos by ${}^{37}\text{Cl}$ produces 48 keV electrons. The average energy of the p - p solar neutrinos is 265 keV. The threshold energy for neutrino absorption in ${}^{71}\text{Ga}$ is 233 keV. Consequently, the produced electron has a low energy. The de Broglie wavelengths of such electrons are larger than the Bohr radii of the atomic K shells in Cl and Ga, and their energies are similar to the kinetic energies of electrons in the K shells. Consequently, screening of the nuclear charge by atomic electrons and final state interactions (exchange effects, radiative corrections, nuclear recoil against the electronic cloud, etc.) may reduce the absorption cross sections of p - p neutrinos in ${}^{71}\text{Ga}$ (perhaps making room for the expected contribution of ${}^7\text{Be}$ in gallium?) and of ${}^7\text{Be}$ neutrinos in ${}^{37}\text{Cl}$ (perhaps making the solar neutrino observations of Kamiokande and the Homestake experiment compatible; Dar, Shaviv, & Shaviv 1996). It is interesting to note that although final state interactions in tritium beta decay have been studied extensively, they do not explain yet the endpoint spectrum ($E_e \sim 18.6$ keV) and why it yields consistently, in all recent measurements, a negative value for the squared mass of the electron neutrino.

Final state interactions in ${}^{37}\text{Cl}$ and ${}^{71}\text{Ga}$ are expected to be much larger because of their much larger values of Z . Note also that this explanation of the solar neutrino problem implies that experiments such as BOREXINO and HELLAZ will observe the full ${}^7\text{Be}$ solar neutrino flux, while the MSW solution predicts that it will be strongly suppressed.

Even if the ${}^7\text{Be}$ solar neutrino flux is strongly suppressed, it does not yet eliminate standard physics solutions to the solar neutrino problem. For instance, collective plasma physics effects, such as very strong magnetic or electric fields near the center of the Sun, may polarize the plasma electrons and affect the branching ratios (BRs) of electron capture by ${}^7\text{Be}$ (spin $3/2^-$) into the ground state (spin $3/2^-$, $E_{\nu_e} = 0.863$ MeV, BR = 90%) and the excited state (spin $1/2^-$, $E_{\nu_e} = 0.381$ MeV, BR = 10%) of ${}^7\text{Li}$. Since solar neutrinos with $E_{\nu_e} = 0.381$ MeV are below the threshold (0.81 MeV) for capture in ${}^{37}\text{Cl}$ and have a capture cross section in ${}^{71}\text{Ga}$ that is smaller by about a factor of 6 relative to solar neutrinos with $E_{\nu_e} = 0.863$ MeV; therefore, a large suppression in the branching ratio to the ground state can produce large suppressions of the ${}^7\text{Be}$ solar neutrino signals in ${}^{37}\text{Cl}$ and in ${}^{71}\text{Ga}$.

8. THE MSW SOLUTION

Standard solar models, like the one presented in this work, perhaps can explain the results reported by Kamiokande. However, standard physics cannot explain an ${}^{37}\text{Ar}$ production rate in ${}^{37}\text{Cl}$ smaller than that expected from the solar ${}^8\text{B}$ neutrino flux measured by Kamiokande. If the experimental results of Kamiokande and Homestake are interpreted as an evidence for such a situation (e.g., Bahcall 1994, 1995), they do imply new physics beyond the standard particle physics model (Bahcall & Bethe 1993). In that case, an elegant solution to the solar neutrino anomaly is resonant neutrino flavor conversion in the Sun, proposed first by Mikheyev & Smirnov (1985) (see also Wolfenstein 1978, 1979). Many authors have carried out extensive calculations to determine the neutrino mixing parameters, which can bridge between the predictions of the standard solar models and the solar neutrino observations. They found a neutrino mass difference $\Delta m^2 \sim 0.7 \times 10^{-5}$ eV² and a neutrino mixing of $\sin^2 2\theta \approx 0.5 \times 10^{-2}$ can solve the solar neutrino problem (see, e.g., Krastev & Petcov 1993; Castellani et al. 1994; Hata et al. 1994; Kwong & Rosen 1994; Berezinsky et al. 1994). In fact, these parameters can be found from simple analytical considerations: As we have seen, the results of GALLEX and SAGE can be predicted directly from the p - p flux, which is fixed by the solar luminosity, and the ${}^8\text{B}$ flux measured by Kamiokande, if GALLEX and SAGE are blind to all other neutrinos. This blindness may be due to flavor conversion of these neutrinos. The resonance condition for flavor conversion in the Sun is

$$n_e = n_e^{\text{res}} = \frac{\Delta m^2 \cos 2\theta}{2\sqrt{2}G_F E_\nu} \approx \frac{\Delta m^2}{2\sqrt{2}G_F E_\nu}, \quad (21)$$

for small mixing angles. Solar p - p neutrinos, whose maximum energy is 0.42 MeV, do not encounter resonance density if the resonance density for $E_\nu = 0.42$ is larger than the central electron density in the Sun. The 0.861 MeV ${}^7\text{Be}$ solar neutrinos, and all the other solar neutrinos that are more energetic, encounter a resonance density in the Sun and suffer a resonance flavor conversion if the resonance

condition is already satisfied for a 0.861 MeV neutrinos. The electron density at the center of the Sun is $n_e \approx 6 \times 10^{25} \text{ cm}^{-3}$, and the last two conditions together with equation (21) yield

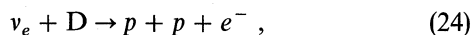
$$0.5 \times 10^6 \text{ eV}^2 \leq \Delta m^2 \leq 1 \times 10^6 \text{ eV}^2. \quad (22)$$

The probability of flavor conservation is given approximately by (e.g., Parke 1986; Dar et al. 1987) $P(\nu_e \rightarrow \nu_e) \approx e^{-\epsilon/E_\nu}$, where

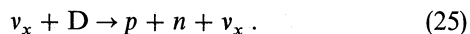
$$\epsilon = \frac{\pi H \Delta m^2 \sin^2 \theta}{4 \cos 2\theta} \approx \frac{\pi H \Delta m^2 \theta^2}{4}; \quad (23)$$

H is the solar scale height at the resonance. Thus, we see that the suppression of the solar ν_e flux can still be adjusted by the choice of the mixing angle θ . A suppression factor of $P \approx e^{-1}$ at the most effective solar neutrino energies (~ 10 MeV) in the chlorine detector yields a suppression factor of e^{-10} at $E_\nu \sim 1$ MeV. Such a suppression and $\Delta m^2 \approx 0.75 \times 10^{-5} \text{ eV}^2$ yield a mixing parameter $\sin^2 2\theta \approx 0.5 \times 10^{-2}$.

Are neutrino oscillations responsible for the solar neutrino anomaly? The answer may be provided by two experiments planned to begin collecting data in 1966; The Sudbury Neutrino Observatory (SNO) will detect two neutrino interactions in 1000 tons of heavy water:



and



If more solar neutrinos are detected via the second reaction (which is blind to the neutrino flavor) than via the first reaction (in which only ν_e values can contribute), it would provide evidence that some solar ν_e values have changed their flavor before reaching the detector. The total solar neutrino flux will also be measured at SNO by elastic scattering on electrons in the light water shield. The expected counting rate in the 1000 tons of heavy water of SNO is about 10 per day! The Superkamiokande experiment will utilize 50,000 tons of high-purity light water and will enhance the counting rate of solar neutrinos in Kamiokande by about a factor of 30. It should have enough statistics to detect the change in the energy spectrum of the high-energy ^8B solar neutrinos predicted by the MSW (Mikheyev & Smirnov 1985; Wolfenstein 1978) solution to the solar neutrino problem.

9. SUMMARY AND CONCLUSIONS

The results of the four pioneering solar neutrino experiments confirm that the Sun derives its energy by fusion of hydrogen into helium in its core. This is a great triumph both for experimental and theoretical physics. The reliability of the results from these difficult and ingenious experiments is supported by their consistency, and recently, most convincingly, by the GALLEX chromium source experiment. The capture rates of solar neutrinos measured by GALLEX and SAGE are above the minimal rates expected from the solar luminosity and the conservation of lepton flavor. The ^8B solar neutrino flux predicted by our improved standard solar model, which was described in this paper, is consistent, within the theoretical and experimental uncertainties, with the solar neutrino observations at Homestake and Kamiokande. However, the experimental

results from the four solar neutrino experiments seem to suggest that the flux of ^7Be solar neutrinos at Earth is much smaller than that predicted by the standard solar models, including our improved SSM which includes pre-main-sequence evolution, element diffusion, partial ionization effects, and all possible nuclear reactions between the main elements, uses updated values for the initial solar element abundances, the solar age, the solar luminosity, the nuclear reaction rates, and the radiative opacities, and does not impose either nuclear equilibrium or complete ionization. Solutions to the solar neutrino problem that do not invoke neutrino properties beyond the standard electroweak model are not ruled out.

The solar neutrino problem may be a terrestrial problem. The neutrino capture cross sections near threshold in the radiochemical experiments may be different from the calculated cross sections (Dar et al. 1996). The inferred solar neutrino fluxes from the GALLEX and HOMESTAKE experiments may be different from the true solar neutrino fluxes. They do not establish beyond doubt that there is a real ^7Be solar neutrino deficit. Perhaps future experiments such as BOREXINO and HELLAZ will be able to establish that.

The solar neutrino problem may be an astrophysical problem. The deviations of the experimental results from those predicted by the standard solar models may reflect the approximate nature of the standard solar models (which neglect, or treat only approximately, many effects and do not explain yet solar activity or the surface depletion of lithium, beryllium, and boron relative to their meteoritic values, which may or may not be relevant to the solar neutrino problem). Improvements of the standard solar model should continue. In particular, dense plasma effects on nuclear reaction rates and radiative opacities, which are not well understood, may strongly affect the SSM predictions and should be studied further, both theoretically and experimentally. Relevant information may be obtained from studies of thermonuclear plasmas in inertial confinement experiments. Useful information may also be obtained from improved data on screening effects in low-energy nuclear cross sections of ions, atomic beams, and molecular beams incident on a variety of gas, solid, and plasma targets.

Better knowledge of low-energy nuclear cross sections is badly needed. Measurement of crucial low-energy nuclear cross sections by new methods, such as measurements of the cross sections for the radiative captures $p + ^7\text{Be} \rightarrow ^8\text{B} + \gamma$ and $^3\text{He} + ^4\text{He} \rightarrow ^7\text{Be} + \gamma$ by photodissociation of ^8B and ^7Be in the Coulomb field of heavy nuclei, are highly desirable.

The ^{37}Ar production rate in ^{37}Cl may indeed be smaller than that expected from the flux of standard solar neutrinos as measured by electron scattering in the Kamiokande experiment. In that case, neutrino oscillations, and in particular the MSW effect, may be the correct solution to the solar neutrino problem. Only future experiments, such as SNO, Superkamiokande, BOREXINO, and HELLAZ, will be able to supply a definite proof that nature has made use of this beautiful effect.

The authors would like to thank an anonymous referee for very useful comments. This research was supported in part by the Technion Fund for Promotion of Research.

REFERENCES

- Abdurashitov, J. N., et al. 1995, Nucl. Phys. B, Proc. Suppl., 38, 60
 Alexander, D. R., Ryma, R. L., & Johnson, H. R. 1983, ApJ, 272, 773
 Anders, E., & Grevesse, N. 1989, Geochim. Cosmochim. Acta, 53, 197
 Anselmann, P., et al. 1995a, Nucl. Phys. B, Proc. Suppl., 38, 68
 ———. 1995b, Phys. Lett. B, 342, 440
 Athanassopoulos, C., et al. 1995, Phys. Rev. Lett., 75, 2650
 Aufderheide, M. B., et al. 1994, Phys. Rev. C, 49, 678
 Bahcall, J. N. 1989, Neutrino Astrophysics (Cambridge: Cambridge Univ. Press)
 ———. 1994, Phys. Lett. B, 338, 276
 ———. 1995, Nucl. Phys. B, Proc. Suppl., 38, 98
 Bahcall, J. N., & Bethe, H. 1991, Phys. Rev. D, 44, 2962
 ———. 1993, Phys. Rev. D, 47, 1298
 Bahcall, J. N., & Loeb, A. 1990, ApJ, 360, 267
 Bahcall, J. N., & Pinsonneault, M. 1992, Rev. Mod. Phys., 64, 885 (BP92)
 ———. 1995, Rev. Mod. Phys., 67, 781 (BP95)
 Bahcall, J. N., & Ulrich, R. K. 1988, Rev. Mod. Phys., 60, 297
 Barish, B. C. 1995, Nucl. Phys. B, Proc. Suppl., 38, 343
 Barker, F. C., & Spear, R. H. 1986, ApJ, 307, 847
 Berezhinsky, V. 1994, Comments Nucl. Part. Phys., 21, 249
 Berezhinsky, V., et al. 1994, Phys. Lett., 341, 38
 Bethe, H. 1939, Phys. Rev., 55, 103
 Bludman, S. A., et al. 1993, Phys. Rev. D, 47, 1298
 Castellani, V., et al. 1994, Phys. Lett. B, 324, 425
 Caughlan, G. R., & Fowler, W. A. 1988, Atomic Data Nucl. Data Tables, 40, 283
 Christensen-Dalsgaard, J. 1994, Europhys. News, 25, 71
 Christensen-Dalsgaard, J., et al. 1993, ApJ, 403, L75
 Clayton, D. 1968, Principles of Stellar Evolution & Nucleosynthesis (New York: McGraw-Hill)
 Cleveland, B. T., et al. 1995, Nucl. Phys. B, Proc. Suppl., 38, 47
 Cox, A. N., Guzik, J. A., & Kidman, R. B. 1989, ApJ, 342, 1187
 Dar, A. 1993, in Particles and Cosmology, ed. E. N. Alexyev et al. (Singapore: World Scientific), 3
 Dar, A., et al. 1987, Phys. Rev. D, 35, 3607
 Dar, A., & Nussinov, S. 1991, Particle World, 2, 117
 Dar, A., & Shaviv, G. 1994, in Proc. VI Int. Conf. on Neutrino Telescopes, ed. M. Baldo-Ceolin (Padua: Univ. Padua), 303, (DS94)
 Dar, A., Shaviv, G., & Shaviv, N. 1996, in preparation
 Dawarakanath, M. R., & Winkler, H. 1971, Phys. Rev. C, 4, 1532
 Descouvemont, P., & Baye, D. 1994, Nucl. Phys. A, 567, 341
 Dzitko, H., et al. 1995, ApJ, 447, 428
 Engstler, S., et al. 1988, Phys. Lett. B, 202, 179
 Filippone, B. W., et al. 1983, Phys. Rev. C, 28, 2222
 Gai, M. 1995, Nucl. Phys. B, Proc. Suppl., 38, 77
 Geiss, J. 1993, in Origin and Evolution of the Elements, ed. N. Prantzos et al. (Cambridge: Cambridge Univ. Press), 89
 Goldsmith, S., et al. 1984, Phys. Rev., A30, 2775
 Gopel, C. et al. 1994, Earth Sci. Lett., 121, 153
 Gorres, J., Wiescher, M., & Rolf, C. 1989, ApJ, 343, 365
 Greife, U., et al. 1994, Nucl. Instrum. Methods A, 350, 327
 Grevesse, N. 1991, A&A, 242, 488
 Grevesse, N., & Noels, A. 1993a, in Origin and Evolution of the Elements, ed. N. Prantzos et al. (Cambridge: Cambridge Univ. Press), 15
 ———. 1993b, Phys. Scr., T47, 133
 Grevesse, N., et al. 1990, A&A, 232, 225
 Guenther, D. B. 1989, ApJ, 339, 1156
 Hata, N., et al. 1994, Phys. Rev. D, 49, 3622
 Hata, N., & Langacker, P. (1995), Phys. Rev. D, 52, 420
 Hernandez, E. P., & Christensen-Dalsgaard, J. 1994, MNRAS, 269, 475
 Hickey, J. R., et al. 1982, J. Sol. Energy, 29, 125
 Hilgemeier, M., et al. 1988, Z. Phys. A, 329, 243
 Hill, J. E. 1995, Phys. Rev. Lett., 75, 2654
 Iben, I., Jr., Fujimoto, M. Y., & MacDonald, J. 1992, ApJ, 388, 521
 Johnson, C. W., et al. 1992, ApJ, 392, 320
 Kamionkowski, M., & Bahcall, J. 1994, ApJ, 420, 884
 Kavanagh, R. W. 1960, Nucl. Phys., 15, 411
 Kim, Y. E., et al. 1995, Nucl. Phys. B, Proc. Suppl., 38, 293
 Kovetz, A., & Shaviv, G. 1994, ApJ, 426, 787
 Krastev, P. I., & Petcov, S. T. 1993, Phys. Lett. B, 299, 99
 Krauss, A., et al. 1987, Nucl. Phys. A, 467, 273
 Krawinkel, H., et al. 1982, Z. Phys. A, 304, 307
 Kubono, S., et al. 1989, ApJ, 344, 460
 Kwong, W., & Rosen, S. 1994, Phys. Rev. Lett., 73, 369
 Lambert, D. L. 1978, MNRAS, 182, 249
 Langacker, P. 1995, Nucl. Phys. B, Proc. Suppl., 38, 152
 Langanke, K. 1991, in Nuclei, in the Cosmos, ed. H. Oberhummer (Berlin: Springer-Verlag), 61
 Lee, R. B., et al. 1991, Metrologica, 28, 265
 Linsky, J. L., et al. 1993, ApJ, 402, 694
 Louis, W. C. 1995, Nucl. Phys. B, Proc. Suppl., 38, 229
 Mihalas, D. 1978, Stellar Atmospheres (San Francisco: W. H. Freeman & Co.)
 Mikheyev, P., & Smirnov, A. Yu. 1985, Yad. Fiz., 42, 1441
 Motobayashi, T., et al. 1994, Phys. Rev. Lett., 73, 2680
 Noerdlinger, P. D. 1977, A&A, 57, 407
 Osborne, J. L., et al. 1984, Nucl. Phys. A, 419, 115
 Parke, S. J. 1995, Phys. Rev. Lett., 74, 839
 ———. 1986, Phys. Rev. Lett., 57, 1275
 Parker, P. D. 1968, ApJ, 153, L85
 Parker, P. D., & Kavanagh, R. W. 1963, Phys. Rev., 131, 2578
 Particle Data Group. 1992, (Aguilar-Benitez, M., et al.)
 ———. 1994, (Aguilar-Benitez, M., et al.), Phys. Rev. D, 50, 1173
 Press, W. H., et al. 1989, Numerical Recipes (Cambridge: Cambridge Univ. Press)
 Proffitt, C. R. 1994, ApJ, 425, 849
 Proffitt, C. R., & Michaud, G. 1991, ApJ, 380, 238
 Rogers, F. J., & Iglesias, C. A. 1992, ApJS, 79, 57
 Rolfs, C. 1994, Nucl. Phys. B, Proc. Suppl., 35, 334
 Sackman, I. J., et al. 1990, ApJ, 360, 727
 Schramm, D. N., & Shi, X. 1994, Nucl. Phys. B, Proc. Suppl., 35, 321
 Shaviv, G. 1995, Nucl. Phys. B, Proc. Suppl., 38, 81
 Shaviv, G., & Shaviv, N. 1996, ApJ, 468, 433
 Shi, X. D., et al. 1994, Phys. Rev. D, 50, 2414
 Shoppa, T. D., et al. 1993, Phys. Rev. C, 48, 837
 Slattery, W. L., Doolen, G. D., & De Witt, H. H. 1980, Phys. Rev. A, 21, 2087
 Soderblom, D. R., et al. 1994, AJ, 106, 1059
 Sturenburg, S., & Holweger, H. 1990, A&A, 237, 125
 Suzuki, Y. 1995, Nucl. Phys. B, Proc. Suppl., 38, 54
 Suzuki, T. S. et al. 1995, ApJ, 439, L59
 Tilton, G. R. 1988, in Meteorites and the Early Solar System, ed. J. F. Kerridge & M. S. Matthews (Tucson: Arizona Press), 259
 Turck-Chieze, S., et al. 1988, ApJ, 335, 415
 Turck-Chieze, S., & Lopes, I. 1993, ApJ, 408, 347 (TL93)
 Vauclair, S., & Charbonnel, C. 1995, A&A, 295, 715
 Vaughn, F. J., et al. 1970, Phys. Rev. C, 2, 1657
 Wasserburg, G. J., et al. 1995, ApJ, 447, L37
 Wiescher, M., et al. 1989, ApJ, 343, 352
 Wilson, R. C. 1993, in Atlas of Satellite Observations, ed. R. J. Gurney et al. (New York: Cambridge Univ. Press), 5
 Wilson, R. C., & Hudson, H. S. 1988, Nature, 332, 810
 Wolfenstein, L. 1978, Phys. Rev. D, 17, 2369
 ———. 1979, Phys. Rev. D, 20, 2634
 Xu, H. M., et al. 1994, Phys. Rev. Lett., 73, 2027